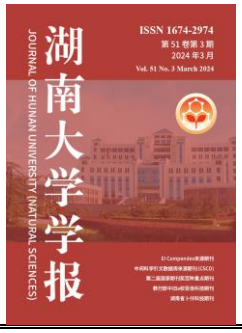

湖南大学学报（自然科学版）
Journal of Hunan University (Natural Sciences)

第 51 卷 第 3 期
2024 年 3 月

Available online at http://jonuns.com/index.php/journal/index

Vol. 51 No. 3
March 2024

Open Access Article

https://doi.org/10.55463/issn.1674-2974.51.3.6

# Comparative Analysis of Finite Difference Methods for Coupled Surface and Subsurface Flows in Extended Shallow Water Equations

**Saeed Ahmed Rajput[1,2]*, Shakeel Ahmed Kamboh[2], Khuda Bux Amur[2]**

[1] Department of Basic Science and Related Study (BS&RS), The University of Larkano, Larkana, Pakistan

[2] Department of Mathematics and Statistics, Quaid-e-Awam University of Engineering, Science and Technology, Nawabshah, Pakistan

* Corresponding author: saeedaahmed@uolrk.edu.pk

*Received: December 5, 2023 / Revised: January 13, 2024 / Accepted: February 23, 2024 / Published: March 29, 2024*

**Abstract:** Numerical simulation of coupled surface and subsurface flows is crucial for modeling equations for flood waves, runoff processes, and tsunami wave propagation with topographical functions in different fields of science and engineering. The shallow water 2D equation was used to model the coupled dynamics of surface and subsurface flows. These equations form a system of coupled nonlinear partial differential equations. The development of an easy-to-use and robust numerical method to accurately determine fluid motion in this coupled flow scenario, including topographic considerations, is of utmost importance. The numerical simulation results of these equations are obtained explicitly using two numerical methods: the forward time-centered scheme and the Lax-Wendroff method. This study compares the numerical simulation results of the connected region at different time steps. The stability is checked through error analysis. Both methods give identical numerical results, although the Lax-Wendroff method shows a slightly better performance. All these numerical results are obtained using CFL stability criteria.

**Keywords:** extended shallow water equation, forward time central scheme, the Lax-Wendroff method.

# 扩展浅水方程中耦合地表和地下水流的有限差分法比较分析

**摘要：**地表和地下流耦合的数值模拟对于在不同科学和工程领域中利用地形函数建模洪水波、径流过程和海啸波传播方程至关重要。浅水二维方程用于模拟地表和地下流动的耦合动力学。这些方程形成耦合非线性偏微分方程组。开发一种易于使用且稳健的数值方法来准确确定这种耦合流动场景中的流体运动（包括地形考虑）至关重要。这些方程的数值模拟结果是使用两种数值方法明确获得的：前向时间中心格式和拉克斯-温德罗夫方法。本研究比较了不同时间步长的连通区域的数值模拟结果。通过误差分析来检验稳定性。两种方法给出相同的数值结果，尽管拉克斯-温德罗夫方法表现出稍好的性能。所有这些数值结果都是使用节能灯稳定性标准获得的。

**关键词：**扩展浅水方程、正向时间中心方案、拉克斯-温德罗夫方法。

# 1. Introduction

The interaction between surface water flow and ground water flow is natural in water bodies such as rivers, lakes, wetlands, coasts, and oceans. Understanding this interaction is essential for managing water resources, predicting floods, and ecological health. For the surface flow that causes runoff or flood flow, problems emerge, when the water enters the city or village; these problems are in the shape of life lost and other losses [1]. In the mid-19th century, Henry Darcy laid the groundwork for the flow of water through porous media, which is a fundamental idea for understanding groundwater dynamics. The study of these two coupled region flows has grown into the dynamics field with diverse research themes and applications [2–5]. Coupled flow modeling involves the integration of surface flow models with ground water flow models, hydrodynamic models, and numerical flow models. This integration allows the simulation of water movement across the interface between surface and subsurface flows [6–9]. Coupled flow simulations have found a wide range of applications in different hydrological studies and water resource management. Some notable applications include flood wave emergencies, dam breaks, tsunami wave propagation [10-11], and irrigation [12]. The shallow water equations are used for surface flow modeling, whereas for subsurface flow, Richard's equation [13] is used. The shallow water equations also use the porosity parameter of the surface flow that also works as a coupling parameter [14]. Different numerical models are adopted to simulate the coupled behavior of the surface and subsurface water flows. These equations are a set of partial differential equations that describe the flow of water in both domains incorporating various parameters. Other models are also used to describe different types of equations for stable solutions with porosity [15-17]. Numerical simulations of coupled surface and subsurface flows have attracted attention in recent years either for surface flows or both regions. Flouri et al. [18] discussed the method of splitting tsunami and Godunov-type finite difference method, and Lu et al. [19] developed a convergence with improved Lax-Friedrichs method for surface flows. Saiduzzaman and Ray [20] discuss different types of finite difference methods for comparison of 1D and 2D shallow water equations. Using a simple weighted essentially non-oscillatory (SWENO) scheme, Lu et al. [21] proposed a Lax-Wendroff-class procedure with a high-order finite volume. To obtain better numerical simulation results for 1D and 2D surface flows, Yuan et al. [22] developed a finite volume method with complex topography for surface flows. The numerical fluxes were calculated using the HLL Riemann solver. Zoppou and Roberts [23] used a finite volume Riemann solver with the van Leer limiter. Studies [24-25] used a finite difference forward time central scheme for the simulation of overland flow. Kirstetter et al. [26] discuss the Darcy-Weisbach equation, Poiseuille friction, and Manning formula to obtain numerical simulation results, which are compared with experimental work. Garcia and Kahawita [27] developed the Mac-Cormack time-splitting scheme for the simulation of a hydraulic model to obtain numerical results for St. Venant's equations. In the present study, a 2D shallow water equation with the porosity and friction resistance parameters is discussed. Different values of the porosity parameter are analyzed for coupled surface and subsurface regions. Validation results are compared with residual error in different time durations.

# 2. Mathematical Model

A mathematical model is a key point for computational methods. Mathematical model choice depends on the specific field of the study and the characteristics of the system under investigation. Flows in shallow water in 2D are modeled using equations from the shallow water equations, and the Navier-Stokes type equations are used for flows in porous media. Here, by depth integration, the 3D Navier-Stokes type equations can be transformed into forms similar to those of the shallow water equations [14].

$$\frac{\partial h}{\partial t}+\frac{\partial}{\partial x}\left(\frac{hu}{\rho_e}\right)+\frac{\partial}{\partial y}\left(\frac{hv}{\rho_e}\right)=0 \quad (1)$$

$$\frac{1}{\rho_e}\frac{\partial}{\partial t}(hu)+\frac{1}{\rho_e^2}\frac{\partial}{\partial x}\left(hu^2+\frac{gh^2}{2}\right)+\frac{1}{\rho_e^2}\frac{\partial}{\partial y}(huv)=gh\left(S_{0x}-S_{fx}\right)-FD_x \quad (2)$$

$$\frac{1}{\rho_e}\frac{\partial}{\partial t}(hv)+\frac{1}{\rho_e^2}\frac{\partial}{\partial x}(huv)+\frac{1}{\rho_e^2}\frac{\partial}{\partial y}\left(hv^2+\frac{gh^2}{2}\right)=gh\left(S_{0y}-S_{fy}\right)-FD_y \quad (3)$$

where $h$ is the height of the water surface, $u$ and $v$ are the depth-averaged velocity components in the $x$ and $y$ directions, $g$ is the acceleration due to gravity, $S_{0x}$, $S_{fx}$ are the surface gradient and frictional resistance in the $x$ direction, and $S_{0y}$ and $S_{fy}$ are the surface gradient and frictional resistance in the $y$ direction, $FD_x$ and $FD_y$ are the external force of the body in the $x$ and $y$ directions, $\rho_e$ is the porosity parameter, and $t$ is the time step. Let $h(x,y,t)=z(x,y,t)+b(x,y)$ be the total height from the free surface to the impenetrable bottom.

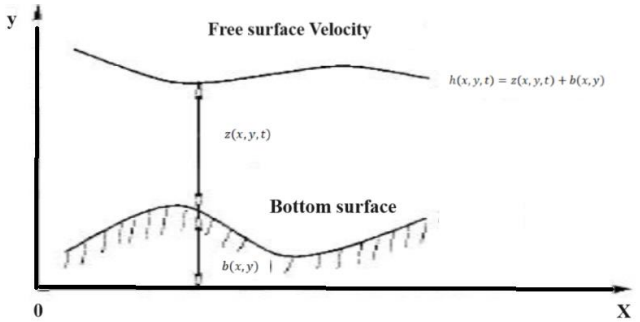


Fig. 1 Numerical domain for the coupled surface and subsurface regions (The authors)

Here are the equations representing either surface flows or subsurface flows, which are obtained by

$$\frac{\partial h}{\partial t}+\frac{\partial}{\partial x}\left(\frac{hu}{\rho_e}\right)+\frac{\partial}{\partial y}\left(\frac{hv}{\rho_e}\right)=0 \quad (4)$$

$$\frac{\partial}{\partial t}(hu)+\frac{1}{\rho_e}\frac{\partial}{\partial x}\left(hu^2+\frac{gh^2}{2}\right)+\frac{1}{\rho_e}\frac{\partial}{\partial y}(huv)=\rho_e gh\left(\beta S_{0x}-S_{fx}\right)-\rho_e FD_x \quad (5)$$

$$\frac{\partial}{\partial t}(hv)+\frac{1}{\rho_e}\frac{\partial}{\partial x}(huv)+\frac{1}{\rho_e}\frac{\partial}{\partial y}\left(hv^2+\frac{gh^2}{2}\right)=\rho_e gh\left(\beta S_{0y}-S_{fy}\right)-\rho_e FD_y \quad (6)$$

where

$$\beta=\begin{cases}1, \rho_e=0,1 \text{ for surface flows}\\ 0,\ 0<\rho_e<1 \text{ for subsurface flows}\end{cases}$$

The bottom slope in $x$ and $y$ directions $S_{0x}$ and $S_{oy}$ is given by [28].

$$S_{0x}=-\frac{\partial b}{\partial x}=-b_x, \text{ and } \mathrm{S_{0y}}=-\frac{\partial b}{\partial x}=-b_y \quad (7)$$

where $b$ is the bottom elevation, and the friction resistance terms $S_{fx}$ and $S_{fy}$ can be defined by Manning's resistance law.

$$S_{fx}=\frac{k^2u\sqrt{u^2+v^2}}{h^{\frac{4}{3}}}, S_{fy}=\frac{k^2v\sqrt{u^2+v^2}}{h^{\frac{4}{3}}}, \quad (8)$$

where $k$ is the Manning roughness coefficient, and the source term $\bar{S}(\bar{U})$ is expressed as

$$\frac{\partial \bar{U}}{\partial t}+\frac{\partial \bar{F}(\bar{U})}{\partial x}+\frac{\partial \bar{G}(\bar{U})}{\partial y}=\bar{S}(\bar{U}), \quad (9)$$

$$\bar{U}_t+\bar{F}_x(\bar{U})+\bar{G}_x(\bar{U})=\bar{S}(\bar{U}), \quad (10)$$

where $\bar{U}=[h,hu,hv]^T$, $\bar{F}(\bar{U}), \bar{G}(\bar{U})$ are the fluxes, and $\bar{S}(\bar{U})$ is the source term defined as

$$\bar{U}=\begin{pmatrix}h\\ hu\\ hv\end{pmatrix},\ \bar{F}(\bar{U})=\begin{pmatrix}\frac{hu}{\rho_e}\\ \frac{1}{\rho_e}\left(hu^2+\frac{gh^2}{2}\right)\\ \frac{huv}{\rho_e}\end{pmatrix}, \quad (11)$$

$$\bar{G}(\bar{U})=\begin{pmatrix}\frac{hv}{\rho_e}\\ \frac{huv}{\rho_e}\\ \frac{1}{\rho_e}\left(hv^2+\frac{gh^2}{2}\right)\end{pmatrix},$$

$$\bar{S}(\bar{U})=\begin{pmatrix}0\\ \rho_e gh\left(-\beta b_x-\frac{k^2u\sqrt{u^2+v^2}}{h^{\frac{4}{3}}}\right)-\rho_e FD_x\\ \rho_e gh\left(-\beta b_y-\frac{k^2v\sqrt{u^2+v^2}}{h^{\frac{4}{3}}}\right)-\rho_e FD_y\end{pmatrix} \quad (12)$$

$$\bar{G}(\bar{U})=\begin{pmatrix}\frac{hv}{\rho_e}\\ \frac{huv}{\rho_e}\\ \frac{1}{\rho_e}\left(hv^2+\frac{gh^2}{2}\right)\end{pmatrix},$$

$$\bar{S}(\bar{U})=\begin{pmatrix}0\\ \rho_e g\left(-h\beta b_x-\frac{k^2u\sqrt{u^2+v^2}}{h^{\frac{1}{3}}}\right)-\rho_e FD_x\\ \rho_e g\left(-\beta hb_y-\frac{k^2v\sqrt{u^2+v^2}}{h^{\frac{1}{3}}}\right)-\rho_e FD_y\end{pmatrix} \quad (13)$$

$$\bar{G}(\bar{U})=\begin{pmatrix}\frac{hv}{\rho_e}\\ \frac{huv}{\rho_e}\\ \frac{1}{\rho_e}\left(hv^2+\frac{gh^2}{2}\right)\end{pmatrix}, \overline{S}(\bar{U})=\begin{pmatrix}0\\ \rho_e g\left(-h\beta b_x-\frac{k^2u\sqrt{u^2+v^2}}{h^{\frac{1}{3}}}\right)-\rho_e FD_x\\ \rho_e g\left(-\beta hb_y-\frac{k^2v\sqrt{u^2+v^2}}{h^{\frac{1}{3}}}\right)-\rho_e FD_y\end{pmatrix}$$

The Jacobian matrix of $\bar{A}(\bar{U})$ of $\bar{F}(\bar{U})$ and $\bar{B}(\bar{U})$ of $\bar{G}(\bar{U})$ are discussed in [23, 29-33]:

$$\bar{A}(\bar{U})=\begin{pmatrix}0 & \frac{1}{\rho_e} & 0\\ \frac{1}{\rho_e}\left(-\frac{U^2}{H}+gH\right) & \frac{2U}{\rho_e H} & 0\\ -\frac{UV}{\rho_e H} & \frac{V}{\rho_e H} & \frac{U}{\rho_e H}\end{pmatrix}$$

$$\bar{B}(\bar{U})=\begin{pmatrix}0 & 0 & \frac{1}{\rho_e}\\ -\frac{UV}{\rho_e H} & \frac{V}{\rho_e H} & \frac{U}{\rho_e H}\\ \frac{1}{\rho_e}\left(-\frac{V^2}{H}+gH\right) & 0 & \frac{2V}{\rho_e H}\end{pmatrix} \quad (14)$$

with the eigenvalues corresponding to matrix $\bar{A}(\bar{U})$ and $\bar{B}(\bar{U})$:

$$\lambda_1=\frac{1}{\rho_e}\left(\frac{U}{H}+\sqrt{\frac{gH}{2}}\right), \lambda_2=\frac{U}{\rho_e H}, \lambda_3=\frac{1}{\rho_e}\left(\frac{U}{H}-\sqrt{\frac{gH}{2}}\right)$$

$$\sigma_1=\frac{1}{\rho_e}\left(\frac{V}{H}+\sqrt{\frac{gH}{2}}\right), \sigma_2=\frac{V}{\rho_e H}, \sigma_3=\frac{1}{\rho_e}\left(\frac{V}{H}-\sqrt{\frac{gH}{2}}\right) \quad (15)$$

where $\lambda_1, \lambda_2$, and $\lambda_3$ are the eigenvalues corresponding to $\bar{A}(\bar{U})$, and $\sigma_1, \sigma_2$, and $\sigma_3$ are eigenvalues crossponding to $\bar{B}(\bar{U})$. Implementation on the MATLAB software considers the following throughout this study:

$$H=h, hu=U, hv=V \quad (16)$$

### 2.1. Initial and Boundary Conditions

$$u(x,y,0)=0, v(x,y,0)=0, h(x,y,0)=1+b(x,y), \quad (17)$$

where

$$b(x,y)=20e^{-0.01[(x-100)^2+(y-15)^2]} \quad (18)$$

$$u(0,y,t)=u_0, u(300,y,t)=u_1, v(x,0,t)=v_0, v(x,50,t)=v_1 \quad (19)$$

where $u_0, u_1, v_0$, and $v_1$ are the left, right, bottom, and top boundary values, respectively. For boundary conditions, the total length $L$ along $x-$ axis is 300 m, the width $W$ along $y-$ axis is 50, and the height is 20 m.

# 3. Numerical Method

The governing equation for the coupled surface and subsurface flow model encompasses three unknown variables, a free surface water level, and two variables originating from the momentum equation. This study employed the cell-centered finite volume method with a rectangular domain to obtain the numerical simulation results for extended shallow water equation (10). This equation is solved using two different finite difference methods.

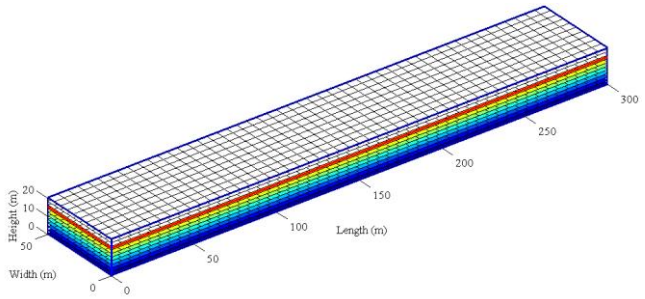


Fig. 2 Numerical domain for surface and subsurface flows (The authors)

### 3.1. Forward Time Central Scheme (FTCS)

The computational domain is divided into a grid of nodes, with the grid point $(i,j)$ representing the spatial coordinates $(x,y)$ and the spacing between the grid points $(\Delta x, \Delta y)$ based on the desired resolution. For the solution of equation (10) employing the explicit forward time central scheme, the domain discretizes into a grid and approximates the derivatives using finite differences. Let us assume a rectangular grid with $\Delta x$ and $\Delta y$ spacing in $x$ and $y$ directions, respectively. Using the forward time scheme, equation (10) is written as

$$\bar{U}_{i,j,n+1} = \bar{U}_{i,j,n} + \frac{\Delta t}{2\Delta x}\left(\bar{F}_{i+1,j,n} - \bar{F}_{i-1,j,n}\right) + \frac{\Delta t}{2\Delta y}\left(\bar{G}_{i,j+1,n} - \bar{G}_{i,j-1,n}\right) + \Delta t \bar{S}_{i,j,n} \quad (20)$$

$$\bar{U}_{i,j,n+1} = \begin{pmatrix} H_{i,j,n+1} \\ U_{i,j,n+1} \\ V_{i,j,n+1} \end{pmatrix}, \bar{U}_{i,j,n} = \begin{pmatrix} H_{i,j,n} \\ U_{i,j,n} \\ V_{i,j,n} \end{pmatrix} \quad (21)$$

$$\bar{F}_{i+1,j,n}(\bar{U}) = \begin{pmatrix} \frac{\left(\frac{U}{H}\right)_{i+1,j,n}}{\rho_e} \\ \frac{1}{\rho_e}\left(\left(\frac{U^2}{H}\right)_{i+1,j,n} + \frac{g}{2}(H^2)_{i+1,j,n}\right) \\ \frac{1}{\rho_e}\left(\frac{UV}{H}\right)_{(i+1,j,n)} \end{pmatrix},$$

$$\bar{F}_{i-1,j,n}(\bar{U}) = \begin{pmatrix} \frac{\left(\frac{U}{H}\right)_{i-1,j,n}}{\rho_e} \\ \frac{1}{\rho_e}\left(\left(\frac{U^2}{H}\right)_{i-1,j,n} + \frac{g}{2}(H^2)_{i-1,j,n}\right) \\ \frac{1}{\rho_e}\left(\frac{UV}{H}\right)_{(i-1,j,n)} \end{pmatrix} \quad (22)$$

$$\bar{G}_{i,j+1,n}(\bar{U}) = \begin{pmatrix} \frac{\left(\frac{V}{H}\right)_{i,j+1,n}}{\rho_e} \\ \frac{1}{\rho_e}\left(\frac{UV}{H}\right)_{(i,j+1,n)} \\ \frac{1}{\rho_e}\left(\left(\frac{V^2}{H}\right)_{i,j+1,n} + \frac{g}{2}(H^2)_{i,j+1,n}\right) \end{pmatrix},$$

$$\bar{G}_{i,j-1,n}(\bar{U}) = \begin{pmatrix} \frac{\left(\frac{V}{H}\right)_{i,j-1,n}}{\rho_e} \\ \frac{1}{\rho_e}\left(\frac{UV}{H}\right)_{(i,j-1,n)} \\ \frac{1}{\rho_e}\left(\left(\frac{V^2}{H}\right)_{i,j-1,n} + \frac{g}{2}(H^2)_{i,j-1,n}\right) \end{pmatrix} \quad (23)$$

$$\bar{S}_{i,j,n}(\bar{U}) = \begin{pmatrix} 0 \\ \rho_e g\left(-H_{i,j,n}\beta\left(\frac{b_{i+1,j}-b_{i-1,j}}{2\Delta x}\right) - \frac{k^2\left(\frac{U}{H}\right)_{i,j,n}\sqrt{\left(\frac{U}{H}\right)^2_{i,j,n}+\left(\frac{V}{H}\right)^2_{i,j,n}}}{H^{1/3}_{i,j,n}}\right) - \rho_e F D_x \\ \rho_e g\left(-\beta\left(\frac{b_{i,j+1}-b_{i,j-1}}{2\Delta y}\right)H_{i,j,n} - \frac{k^2\left(\frac{V}{H}\right)_{i,j,n}\sqrt{\left(\frac{U}{H}\right)^2_{i,j,n}+\left(\frac{V}{H}\right)^2_{i,j,n}}}{H^{1/3}_{i,j,n}}\right) - \rho_e F D_y \end{pmatrix} \quad (24)$$

where $(i,j)$ represents the grid indices in the $x$ and $y$ directions, $n \in \mathbb{Z}^+$ is the time step index, and $\bar{F}(\bar{U})$ and $\bar{G}(\bar{U})$ are the horizontal and vertical fluxes in the $x$ and $y$ directions, which depend on the current values of $H$, $U$, and $V$. The finite difference central scheme is applied to compute the fluxes at the current time step $(n)$ and the next time step $(n+1)$. The 2D extended shallow water equations are solved using an advance central system [34].

$$\Delta t < c.\frac{\min(\Delta x, \Delta y)}{2\max\left(\frac{1}{\rho_e}\left(\frac{U}{H}\pm\sqrt{\frac{gH}{2}}\right), \frac{1}{\rho_e}\left(\frac{V}{H}\pm\sqrt{\frac{gH}{2}}\right)\right)} \quad (25)$$

where $c$ is the CFL condition $0 < c < 1$.

### 3.2. The Finite Difference Lax-Wendroff Method

Consider the uniform rectangular mesh grid at the points $(x_i, y_j)$ with the constant grid step $\Delta x = x_{i+1} - x_i$, $\Delta y = y_{i+1} - y_i$ and the dual meshes at the center points given as $\left(x_{i+\frac{1}{2}}, y_{i+\frac{1}{2}}\right) = \left(\frac{\Delta x}{2} + x_i, \frac{\Delta}{2} + y_i\right)$, discretization of equation (10) uses the Lax-Wendroff method. The first half step of the method is as follows [35]:

$$\bar{U}_{i+\frac{1}{2},j+\frac{1}{2},n+\frac{1}{2}} = \frac{1}{4}\left(\bar{U}_{i,j,n} + \bar{U}_{i+1,j,n} + \bar{U}_{i,j+1,n} + \bar{U}_{i+1,j+1,n}\right) + \frac{\Delta t}{2\Delta x}\left(\bar{F}_{i+1,j+1,n} - \bar{F}_{i,j+1,n}\right) + \frac{\Delta t}{2\Delta y}\left(\bar{G}_{i+1,j+1,n} - \bar{G}_{i+1,j,n}\right) + \Delta t \bar{S}_{i,j,n} \quad (26)$$

where

$$\bar{U}_{i+\frac{1}{2},j+\frac{1}{2},n+\frac{1}{2}} = \begin{pmatrix} H_{i+\frac{1}{2},j+\frac{1}{2},n+\frac{1}{2}} \\ U_{i+\frac{1}{2},j+\frac{1}{2},n+\frac{1}{2}} \\ V_{i+\frac{1}{2},j+\frac{1}{2},n+\frac{1}{2}} \end{pmatrix} \quad (27)$$

The second step of the method is defined below,

which completes the time step by using the values computed from the first half step.

$$\bar{U}_{i,j,n+1} = \bar{U}_{i,j,n} - \frac{\Delta t}{2\Delta x}\left(\bar{F}_{i+\frac{1}{2},j+\frac{1}{2},n+\frac{1}{2}} - \bar{F}_{i-\frac{1}{2},j+\frac{1}{2},n+\frac{1}{2}}\right) - \frac{\Delta t}{2\Delta y}\left(\bar{G}_{i+\frac{1}{2},j+\frac{1}{2},n+\frac{1}{2}} - \bar{G}_{i-\frac{1}{2},j-\frac{1}{2},n+\frac{1}{2}}\right) + \Delta t \bar{S}^{n}_{i,j} \quad (28)$$

$$\bar{F}_{i+\frac{1}{2},j+\frac{1}{2},n+\frac{1}{2}}(\bar{U}) = \begin{pmatrix} \frac{\left(\frac{U}{H}\right)_{i+\frac{1}{2},j+\frac{1}{2},n+\frac{1}{2}}}{\rho_e} \\ \frac{1}{\rho_e}\left(\left(\frac{U^2}{H}\right)_{i+\frac{1}{2},j+\frac{1}{2},n+\frac{1}{2}} + \frac{g}{2}(H^2)_{i+\frac{1}{2},j+\frac{1}{2},n+\frac{1}{2}}\right) \\ \frac{1}{\rho_e}\left(\frac{UV}{H}\right)_{\left(i+\frac{1}{2},j+\frac{1}{2},n+\frac{1}{2}\right)} \end{pmatrix},$$

$$\bar{F}_{i-\frac{1}{2},j+\frac{1}{2},n+\frac{1}{2}}(\bar{U}) = \begin{pmatrix} \frac{\left(\frac{U}{H}\right)_{i-\frac{1}{2},j+\frac{1}{2},n+\frac{1}{2}}}{\rho_e} \\ \frac{1}{\rho_e}\left(\left(\frac{U^2}{H}\right)_{i-\frac{1}{2},j+\frac{1}{2},n+\frac{1}{2}} + \frac{g}{2}(H^2)_{i-\frac{1}{2},j+\frac{1}{2},n+\frac{1}{2}}\right) \\ \frac{1}{\rho_e}\left(\frac{UV}{H}\right)_{\left(i-\frac{1}{2},j+\frac{1}{2},n+\frac{1}{2}\right)} \end{pmatrix}, \quad (29)$$

$$\bar{G}_{i+\frac{1}{2},j+\frac{1}{2},n+\frac{1}{2}}(\bar{U}) = \begin{pmatrix} \frac{\left(\frac{V}{H}\right)_{i+\frac{1}{2},j+\frac{1}{2},n+\frac{1}{2}}}{\rho_e} \\ \frac{1}{\rho_e}\left(\frac{UV}{H}\right)_{i+\frac{1}{2},j+\frac{1}{2},n+\frac{1}{2}} \\ \frac{1}{\rho_e}\left(\left(\frac{V^2}{H}\right)_{i+\frac{1}{2},j+\frac{1}{2},n+\frac{1}{2}} + \frac{g}{2}(H^2)_{i+\frac{1}{2},j+\frac{1}{2},n+\frac{1}{2}}\right) \end{pmatrix},$$

$$\bar{G}_{i+\frac{1}{2},j-\frac{1}{2},n+\frac{1}{2}}(\bar{U}) = \begin{pmatrix} \frac{\left(\frac{V}{H}\right)_{i+\frac{1}{2},j-\frac{1}{2},n+\frac{1}{2}}}{\rho_e} \\ \frac{1}{\rho_e}\left(\frac{UV}{H}\right)_{i+\frac{1}{2},j-\frac{1}{2},n+\frac{1}{2}} \\ \frac{1}{\rho_e}\left(\left(\frac{V^2}{H}\right)_{i+\frac{1}{2},j-\frac{1}{2},n+\frac{1}{2}} + \frac{g}{2}(H^2)_{i+\frac{1}{2},j-\frac{1}{2},n+\frac{1}{2}}\right) \end{pmatrix} \quad (30)$$

## 4. Results and Discussion

This study presents numerical results for the selected model of coupled surface and subsurface flows. These results are achieved using the two numerical finite difference methods. For both numerical methods, the results were considered in the given computation domain with the same initial and boundary conditions. Simulation results were obtained numerically by using computer programing software MATLAB. After discussing the numerical results with the aforementioned conditions, a comparison of the numerical results of these applied numerical methods in coupled surface and subsurface flow is presented. The numerical results are drawn for the fixed parameters, $k = 0.01$, $FD_x = -0.1$, $FD_y = -0.1$, $g = 9.8$, $CFL = 0.001$, $\beta = 0$, and $\rho_e = 1$ for the surface flow region and $\rho_e = 0.2$ for the subsurface flow region using the Lax-Wendroff method and FTCS.

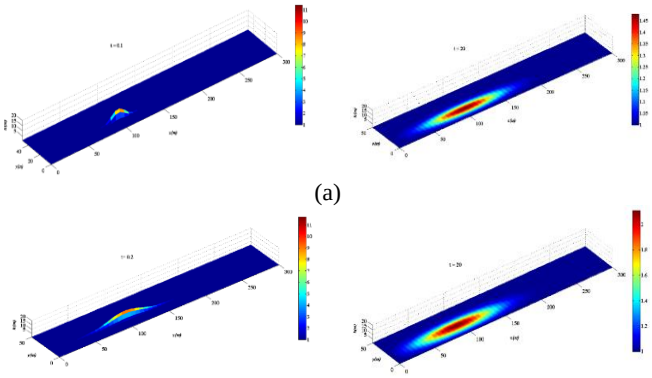

(a)

(b)

Fig. 3 Surface flow for the height function $h(x, y, t)$ by using (a) the Lax-Wendroff method and (b) FTCS (The authors)

The mesh displacement is incorporated into the height function $h(x, y, t)$ for the specific time $t$. It is found that without the source term, the height function decreases, and the wave decreases in height and produces external momentum as the duration increases using two methods for the surface flow region.

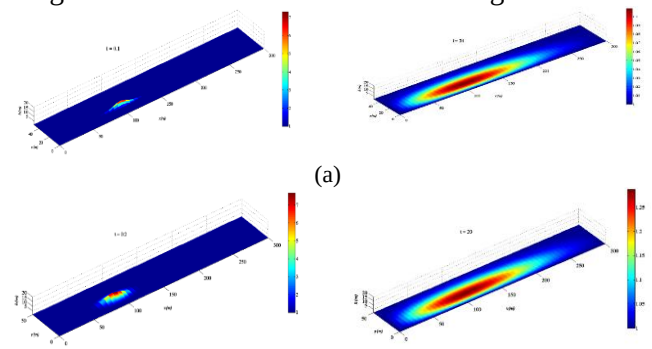

(a)

(b)

Fig. 4 Subsurface flow for the height function $h(x, y, t)$ by using (a) the Lax-Wendroff method and (b) FTCS (The authors)

These graphs indicate that extending the time duration to $t = 20$ leads to the observable reduction in the height from $h = 7$ to $h = 1.1$, with the fixed parameters for the study of the subsurface flow region.

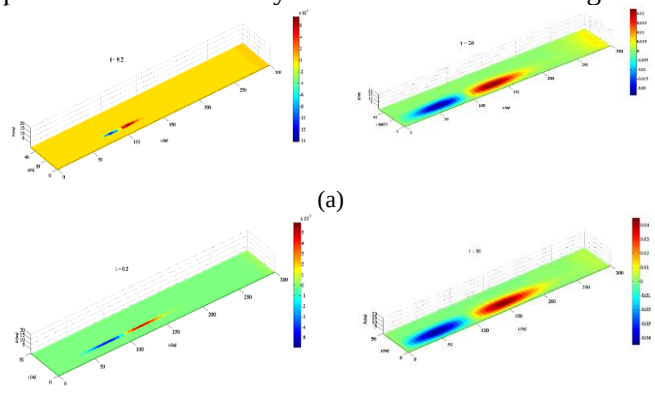

(a)

(b)

Fig. 5 Surface flow for the velocity function $u(x, y, t)$ by using (a)

the Lax-Wendroff method and (b) FTCS (The authors)

Through all computational analyses, it was observed that the vertical displacement of the surface flow area (water height) decreases as the slope of the bottom increases; however, the velocity of the water increases. On the contrary, the increase in the slope friction factor decreases the velocity function $u(x, y, t)$.

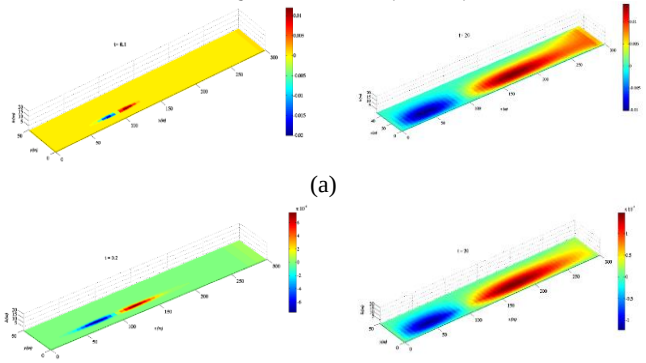

(a)

(b)

Fig. 6 Subsurface flow for the velocity function $u(x, y, t)$ by using (a) the Lax-Wendroff method and (b) FTCS (The authors)

These computational analyses reveal the numerical results for the subsurface flow regions for the velocity function in $x$ direction. It has been observed that as the bottom bed slope increases for the subsurface flow region, the vertical height of the water flow decreases, but it is noted that the velocity discharge rate increases through the cross-sectional area. The discharge rate and cross-sectional area are greater than those in the surface flow region.

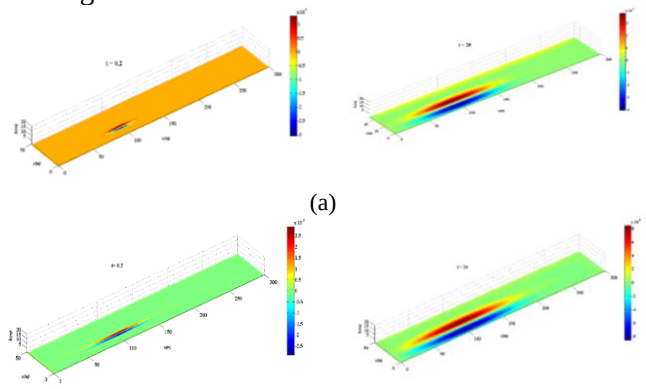

(a)

(b)

Fig. 7 Surface flow for the velocity function $v(x, y, t)$ by using (a) the Lax-Wendroff method and (b) FTCS (The authors)

The analyses show that as time increases, keeping the other terms unchanged, the vertical movement of the water decreases for the velocity function $v(x, y, t)$ for the surface flow region. This phenomenon occurred due to the impact of the applied wave leading to the collapse of the water height and the generation of momentum.

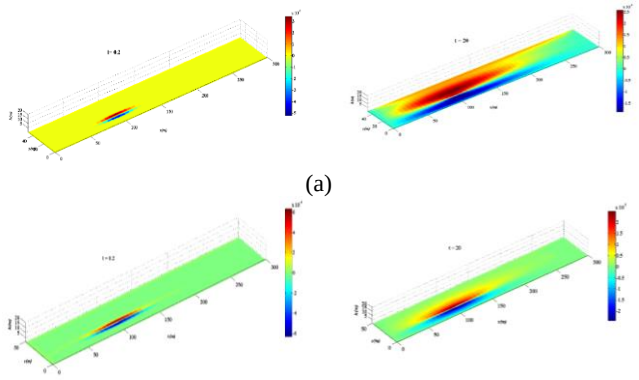

(a)

(b)

Fig. 8 Subsurface flow for the velocity function $v(x, y, t)$ by using (a) the Lax-Wendroff method and (b) FTCS (The authors)

The above figures show the graphical simulation result for velocity function $v$ for the subsurface flow region using both methods. It is observed that the vertical displacement of the velocity decreases with increasing time in the same manner as in the surface flow region. In the subsurface flow region, the discharge rate is greater than that in the surface flow region, and the vertical height of the fluid is less than that in the surface flow region.

### 4.1. Error Analysis

When conducting error analysis for the 2D coupled surface and subsurface flow region, an exact solution is required. However, obtaining precise solutions for these interconnected equations proves to be exceptionally challenging, leading many researchers to opt for many numerical schemes to obtain numerical simulation results. The complexity of the coupled systems often makes it impractical or infeasible to find the exact solution, which emphasizes the reliance on the numerical approach for obtaining valuable information and accurate predictions. Suppose $N$ denote the total number of cells and $h_{i,j,n}$ denote the numerical solution for the height function $h$ at $n$ time step in cells $i, j = 1,2, \ldots N$, similarly, let $u_{i,j,n}$ and $v_{i,j,n}$ denote the numerical solution of velocity function $u$ and $v$. Furthermore, due to the unavailability of the exact solution, consider the next time step solution for the height function as $h_{i,j,n+1}$ in $(i, j)$ cell similarly for velocity function $u_{i,j,n+1}$ and $v_{i,j,n+1}$. Consider the $L_1$ and $L_\infty$ for the evaluation function $h(x, y, t)$ and the residual error for the velocity functions as

$$L_1(h) = \frac{1}{N}\sum_{i,j=1}^{N}\left|h_{i,j,n+1} - h_{i,j,n}\right| \quad (31)$$

$$L_\infty(h) = \max_{i,j=1,2\ldots N}\left|h_{i,j,n+1} - h_{i,j,n}\right| \quad (32)$$

$$R.E = \frac{1}{N}\sum_{i,j=1}^{N}\left|((u_{i,j,n+1} - u_{i,j,n}) + (v_{i,j,n+1} - v_{i,j,n}))/\ (\Delta x + \Delta y)\right| \quad (33)$$

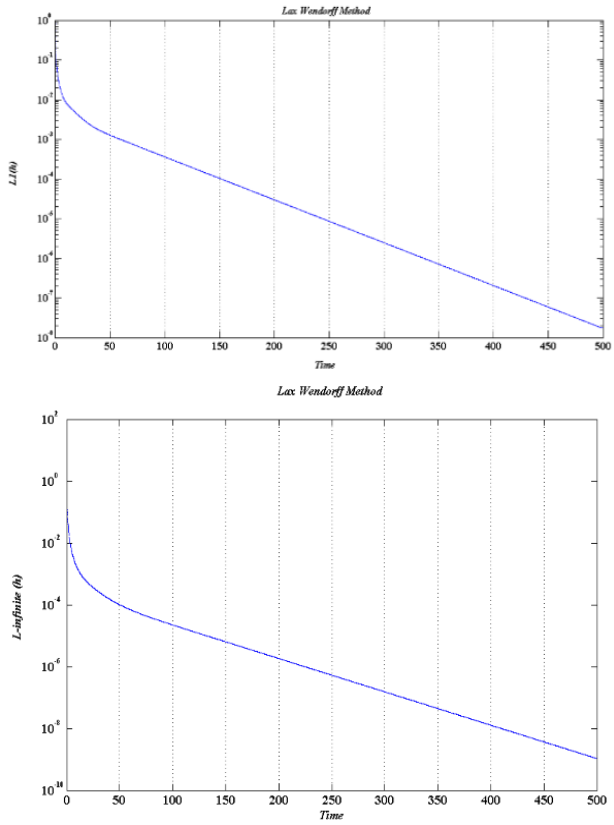


Fig. 9 $L_1$ and $L_\infty$ errors for the height function $h$ by using the Lax-Wendroff method with $\rho_e = 0.2,\ \beta = 1, CFL = 0.001, k = 0.01,$ and $g = 9.8$ (The authors)

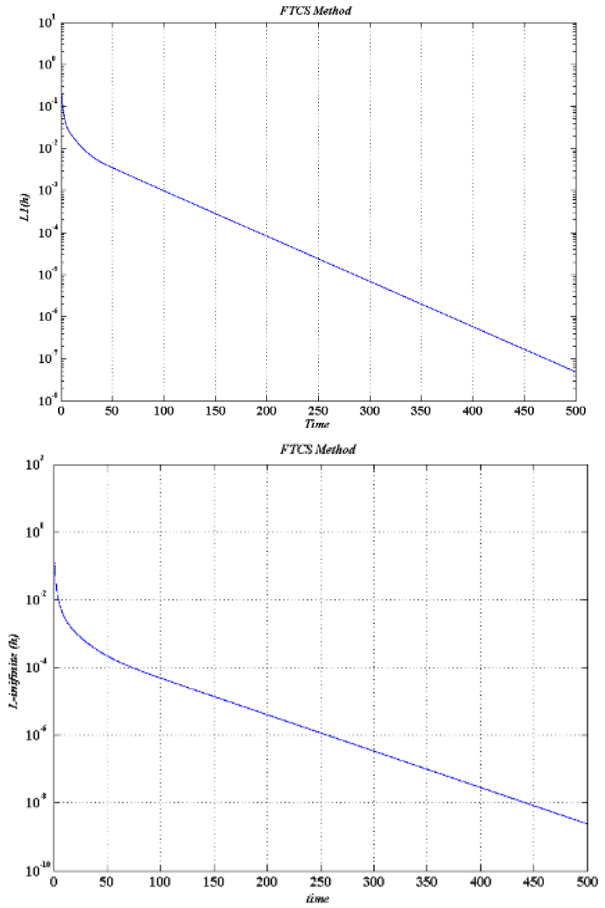


Fig. 10 $L_1$ and $L_\infty$ errors for the height function $h$ by using FTCS with $\rho_e = 0.2,\ \beta = 1, CFL = 0.001, k = 0.01,$ and $g = 9.8$ (The authors)

These figures illustrate $L_1(h)$ and $L_\infty(h)$ computed error for the free surface velocity of the height function using the two distinct methods for the fixed values of the parameters. Upon close examination of these computed errors, it is evident that the Lax-Wendroff method exhibits a smaller error than the FTCS, demonstrating the notable close in errors. However, the Lax-Wendroff method produces more consistent and favorable results than FTCS.

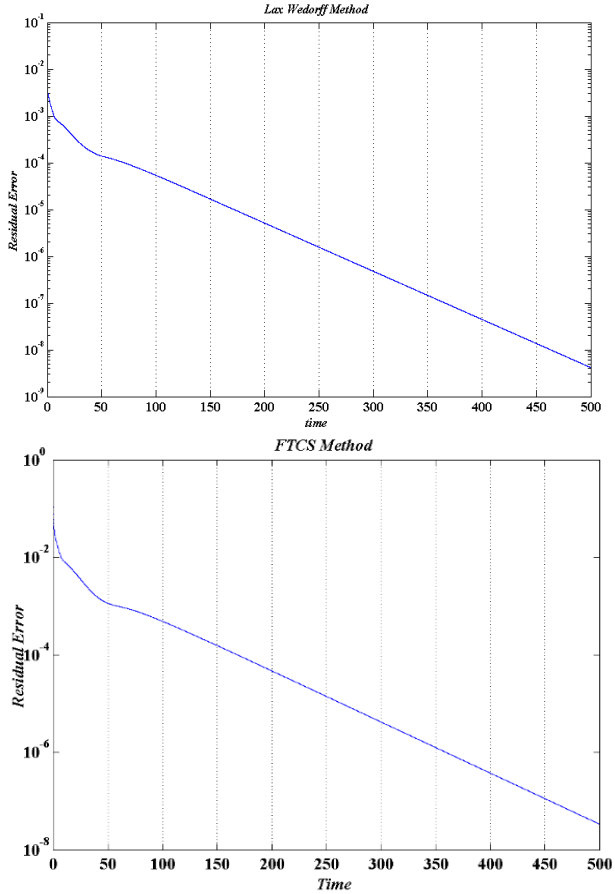


Fig. 11 Residual errors for velocity functions using the Lax-Wendroff and FTCS methods with $\rho_e = 0.2,\ \beta = 1, CFL = 0.001, k = 0.01,$ and $g = 9.8$ (The authors)

The residual error for the velocity function is computed on the basis of these figures for fixed values of the parameters. Both methods are employed for assessing the residual error for the velocity function, which indicates that the Lax-Wendroff method has a small residual error compared to FTCS.

## 5. Conclusion

The main objective of this study was to obtain numerical simulation results for the approximation of two-dimensional extended shallow water equations that include source terms. These equations represent the interaction of the coupled surface and subsurface flow regions. The extended shallow water equation is used to model the interaction between the surface and subsurface flow regions based on the value of $\rho_e$. This approach bypasses the use of the Richard and

Boussinesq equations commonly used for subsurface flow. By integrating $\rho_e$ effects, this modified formulation captures both surface and groundwater behavior without using additional equations related to subsurface flow dynamics. The focus is on the numerical simulation results that provide an accurate portrayal of the complex dynamics of involvement in these systems. From these numerical methods, it has been concluded that the Lax-Wendroff method outperforms FTCS in both speed and accuracy when computed with the same inputs. To ensure the stability of these methods, very small time steps are considered, reducing $CFL$ value to $0.001$ in such instances. This approach is crucial for obtaining the stability of the numerical simulations with the Manning coefficient and source term. Remarkably, both methods provide stable and consistent results even without the Reimann solver and finite volume methods, as long as a small CFL value is used. This research also includes the investigation of other finite difference techniques to obtain numerical simulation results that are available in the literature. In conclusion, the main finding indicates that in the subsurface flow regions, increases in both velocity and cross-sectional area correlated with an escalation of discharge. Numerical simulations reveal direct proportionality between the friction source term, velocities, and vertical displacement of water flow. This relationship illustrates the mutual influence of these factors, emphasizing the importance of considering the velocity, vertical displacement, and friction slope term in the analysis of hydraulic phenomena. Physically, water flowing with a lower slope tends to have a slower velocity than water flowing with a greater slope.

## References

[1] MUJUMDAR P. P. Flood wave propagation: The saint venant equations. *Resonance*, 2001, 6(5): 66-73. https://doi.org/10.1007/BF02839085

[2] DE SCHEPPER G., THERRIEN R., REFSGAARD J. C., and HANSEN A. L. Simulating coupled surface and subsurface water flow in a tile-drained agricultural catchment. *Journal of Hydrology*, 2015, 521: 374-388. https://doi.org/10.1016/j.jhydrol.2014.12.035

[3] OSEI-KUFFUOR D., MAXWELL R. M., and WOODWARD C. S. Improved numerical solvers for implicit coupling of subsurface and overland flow. *Advances in Water Resources*, 2014, 74: 185-195. https://doi.org/10.1016/j.advwatres.2014.09.006

[4] DAVISON J. H., HWANG H. T., SUDICKY E. A., MALLIA D. V., and LIN J. C. Full coupling between the atmosphere, surface, and subsurface for integrated hydrologic simulation. *Journal of Advances in Modeling Earth Systems*, 2018, 10(1): 43-53. https://doi.org/10.1002/2017MS001052

[5] LIANG D., FALCONER R. A., and LIN B. Coupling surface and subsurface flows in a depth averaged flood wave model. *Journal of Hydrology*, 2007, 337(1-2): 147-158. https://doi.org/10.1016/j.jhydrol.2007.01.045

[6] KUMAR A., & PAHAR G. A unified depth-averaged approach for integrated modeling of surface and subsurface flow systems. *Journal of Hydrology*, 2020, 591: 125339. https://doi.org/10.1016/j.jhydrol.2020.125339

[7] BISHT G., HUANG M., ZHOU T., CHEN X., DAI H., HAMMOND G. E., RILEY W. J., DOWNS J. L., LIU Y., and ZACHARA J. M. Coupling a three-dimensional subsurface flow and transport model with a land surface model to simulate stream–aquifer–land interactions (CP v1. 0). *Geoscientific Model Development*, 2017, 10(12): 4539-4562. https://doi.org/10.5194/gmd-10-4539-2017

[8] KUFFOUR B. N., ENGDAHL N. B., WOODWARD C. S., CONDON L. E., KOLLET S., and MAXWELL R. M. Simulating coupled surface–subsurface flows with ParFlow v3. 5.0: capabilities, applications, and ongoing development of an open-source, massively parallel, integrated hydrologic model. *Geoscientific Model Development*, 2020, 13(3): 1373-1397. https://doi.org/10.5194/gmd-13-1373-2020

[9] COON E. T., MOULTON J. D., KIKINZON E., BERNDT M., MANZINI G., GARIMELLA R., LIPNIKOV K., and PAINTER S. L. Coupling surface flow and subsurface flow in complex soil structures using mimetic finite differences. *Advances in Water Resources*, 2020, 144: 103701. https://doi.org/10.1016/j.advwatres.2020.103701

[10] RIESTIANA V. A., SETIYOWATI R., and KURNIAWAN V. Y. Numerical solution of the one dimentional shallow water wave equations using finite difference method: Lax-Friedrichs scheme. *AIP Conference Proceedings*, 2021, 2326: 020022. https://doi.org/10.1063/5.0039545

[11] SETIYOWATI R. A Simulation of Shallow Water Wave Equation Using Finite Volume Method: Lax-Friedrichs Scheme. *Journal of Physics: Conference Series*, 2019, 1306: 012022. https://doi.org/10.1088/1742-6596/1306/1/012022

[12] PANTELAKIS D., ZISSIS T., ANASTASIADOU-PARTHENIOU E., and BALTAS E. Numerical models for the simulation of overland flow in fields within surface irrigation systems. *Water Resources Management*, 2012, 26: 1217-1229. https://doi.org/10.1007/s11269-011-9955-2

[13] RICHARDS L. A. Capillary conduction of liquids through porous mediums. *Journal of Applied Physics*, 1931, 1(5): 318-333. https://doi.org/10.1063/1.1745010

[14] LI Y., YUAN D., LIN B., and TEO F. Y. A fully coupled depth-integrated model for surface water and groundwater flows. *Journal of Hydrology*, 2016, 542: 172-184. https://doi.org/10.1016/j.jhydrol.2016.08.060

[15] BHUTTO A. A., AHMED I., RAJPUT S. A., and SHAH S. A. R. The effect of oscillating streams on heat transfer in viscous magnetohydrodynamic MHD fluid flow. *VFAST Transactions on Mathematics*, 2023, 11(1): 1-16. https://doi.org/10.21015/vtm.v11i1.1386

[16] BHUTTO A. A., SHAH S. F., KHOKHAR R. B., HARIJAN K., and HUSSAIN M. To Investigate Obstacle Configuration Effect on Vortex Driven Combustion Instability. *VFAST Transactions on Mathematics*, 2023, 11(1): 67-82. https://doi.org/10.21015/vtm.v11i1.1411

[17] KHOKHAR R. B., BHUTTO A. A., BHUTTO I. A., MENGAL A., SHAIKH F., and SHAIKH A. A. Numerical Analysis of Non-Newtonian Fluid Flows through an Annulus Occupied with or without Porous Materials. *Balochistan Journal of Engineering & Applied Sciences (BJEAS) HEC Recognized in "Y" Category*, 2023.

[18] FLOURI E. T., KALLIGERIS N., ALEXANDRAKIS G., KAMPANIS N. A., and SYNOLAKIS C. E. Application of a finite difference computational model to the simulation of earthquake generated tsunamis. *Applied Numerical Mathematics,* 2013, 67: 111-125. https://doi.org/10.1016/j.apnum.2011.06.003

[19] LU X., DONG B., MAO B., and ZHANG X. Convergence Improved Lax-Friedrichs Scheme Based Numerical Schemes and Their Applications in Solving the One-Layer and Two-Layer Shallow-Water Equations. *Mathematical Problems in Engineering,* 2015, 2015: 379281. https://doi.org/10.1155/2015/379281

[20] SAIDUZZAMAN M., & RAY S. K. Comparison of Numerical Schemes for Shallow Water Equation. *Global Journal of Science Frontier Research: Mathematics and Decision Sciences,* 2013, 13(4): 28-46. https://www.researchgate.net/profile/Sobuj-Ray/publication/258342122_Comparison_of_Numerical_Schemes_for_Shallow_Water_Equation/links/5882ff55a6fdcc6b790ef1b8/Comparison-of-Numerical-Schemes-for-Shallow-Water-Equation.pdf

[21] LU C., XIE L., and YANG H. The simple finite volume Lax-Wendroff weighted essentially nonoscillatory schemes for shallow water equations with bottom topography. *Mathematical Problems in Engineering,* 2018, 2018, 2652367. https://doi.org/10.1155/2018/2652367

[22] BING Y. U. A. N., JIAN S. U. N., YUAN D. K., and TAO J. H. Numerical simulation of shallow-water flooding using a two-dimensional finite volume model. *Journal of Hydrodynamics, Ser. B,* 2013, 25(4): 520-527. https://doi.org/10.1016/S1001-6058(11)60391-1

[23] ZOPPOU C., & ROBERTS S. Numerical solution of the two-dimensional unsteady dam break. *Applied Mathematical Modelling,* 2000, 24(7): 457-475. https://doi.org/10.1016/S0307-904X(99)00056-6

[24] RAJPUT S. A., KAMBOH S. A., AMUR K. B., MEMON S., and GHOTO A. A. Numerical simulation of 2D shallow water equation with constant external body force by using finite difference method. *VFAST Transactions on Mathematics,* 2023, 11(1): 170-179. https://doi.org/10.21015/vtm.v11i1.1469

[25] KAMBOH S. A., SARBINI I. N., LABADIN J., and EZE M. O. Simulation of 2D Saint-Venant Equations in Open Channel by Using MATLAB. *Journal of IT in Asia,* 2015, 5(1): 15-22. https://doi.org/10.33736/jita.47.2015

[26] KIRSTETTER G., HU J., DELESTRE O., DARBOUX F., LAGRÉE P. Y., POPINET S., FULLANA J. M., and JOSSERAND C. Modeling rain-driven overland flow: Empirical versus analytical friction terms in the shallow water approximation. *Journal of Hydrology,* 2016, 536: 1-9. https://doi.org/10.1016/j.jhydrol.2016.02.022

[27] GARCIA R., & KAHAWITA R. A. Numerical solution of the St. Venant equations with the MacCormack finite-difference scheme. *International Journal for Numerical Methods in Fluids,* 1986, 6(5): 259-274. https://doi.org/10.1002/fld.1650060502

[28] AMIRI S. M., TALEBBEYDOKHTI N., and BAGHLANI A. A two-dimensional well-balanced numerical model for shallow water equations. *Scientia Iranica,* 2013, 20(1): 97-107. https://doi.org/10.1016/j.scient.2012.12.001

[29] ANASTASIOU K., & CHAN C. T. Solution of the 2D shallow water equations using the finite volume method on unstructured triangular meshes. *International Journal for Numerical Methods in Fluids,* 1997, 24(11): 1225-1245. https://doi.org/10.1002/(SICI)1097-0363(19970615)24:11<1225::AID-FLD540>3.0.CO;2-D

[30] KURGANOV A. Finite-volume schemes for shallow-water equations. *Acta Numerica,* 2018, 27: 289-351. https://doi.org/10.1017/S0962492918000028

[31] NAMIO F. T., NGONDIEP E., NTCHANTCHO R., and NTONGA J. C. Mathematical Model of Complete Shallow Water Problem with Source Terms, Stability Analysis of Lax-Wendroff Scheme. *Journal of Theoretical and Computational Science,* 2015, 2(4): 1000132. https://doi.org/10.4172/2376-130x.1000132

[32] LIANG S. J., TANG J. H., and WU M. S. Solution of shallow-water equations using least-squares finite-element method. *Acta Mechanica Sinica,* 2008, 24: 523-532. https://doi.org/10.1007/s10409-008-0151-4

[33] ALCRUDO F., & GARCIA-NAVARRO P. A high-resolution Godunov-type scheme in finite volumes for the 2D shallow-water equations. *International Journal for Numerical Methods in Fluids,* 1993, 16(6): 489-505. https://doi.org/10.1002/fld.1650160604

[34] BRAND S. Parallel Algorithm for Numerical Solution of the Shallow Water Equation. Proceedings of the Czech–Japanese Seminar in Applied Mathematics, Prague, 2006, pp. 25–36. https://geraldine.fjfi.cvut.cz/cjs2006/proc/brand.pdf

[35] WAKJIRA G. T. *Numerical Solution for Flood Propagation Model Using Finite Difference and Finite Volume Methods.* Doctoral thesis, 2017.

**参考文:**

[1] MUJUMDAR P. P. 洪水波传播：圣维南方程。共振，2001，6(5)：66-73。https://doi.org/10.1007/BF02839085

[2] DE SCHEPPER G.、THERRIEN R.、REFSGAARD J. C. 和 HANSEN A. L. 模拟瓷砖排水农业流域中的耦合地表水和地下水流。水文学杂志，2015，521：374-388。https://doi.org/10.1016/j.jHydrol.2014.12.035

[3] OSEI-KUFFUOR D.、MAXWELL R. M. 和 WOODWARD C. S. 改进了地下和地表流隐式耦合的数值求解器。水资源进展，2014，74：185-195。https://doi.org/10.1016/j.advwatres.2014.09.006

[4] DAVISON J. H.、HWANG H. T.、SUDICKY E. A.、MALLIA D. V. 和 LIN J. C. 大气、地表和地下之间的完全耦合，用于综合水文模拟。地球系统模拟进展杂志，2018，10(1)：43-53. https://doi.org/10.1002/2017MS001052

[5] LIANG D., FALCONER R. A., 和 LIN B. 深度平均洪水波模型中地表和地下流的耦合。水文学学报，2007，337(1-2)：147-158.

https://doi.org/10.1016/j.jHydrol.2007.01.045
[6] KUMAR A., & PAHAR G. 用于地表和地下流动系统集成建模的统一深度平均方法。水文学杂志，2020年，591：125339。https://doi.org/10.1016/j.jHydrol.2020.125339
[7] BISHT G., HUANG M., ZHOU T., CHEN X., DAI H., HAMMOND G. E., RILEY W. J., DOWNS J. L., LIU Y., 和 ZACHARA J. M. 耦合三维地下流动和输运模型模拟河流-含水层-土地相互作用的地表模型（CP v1.0）。地学模型开发, 2017, 10(12): 4539-4562. https://doi.org/10.5194/gmd-10-4539-2017
[8] KUFFOUR B. N.、ENGDAHL N. B.、WOODWARD C. S.、CONDON L. E.、KOLLET S. 和 MAXWELL R. M. 使用帕流v3模拟耦合地表-地下流。5.0：开源、大规模并行、集成水文模型的功能、应用程序和持续开发。地学模型开发, 2020, 13(3): 1373-1397. https://doi.org/10.5194/gmd-13-1373-2020
[9] COON E. T.、MOULTON J. D.、KIKINZON E.、BERNDT M.、MANZINI G.、GARIMELLA R.、LIPNIKOV K. 和 PAINTER S. L. 使用模拟有限差分耦合复杂土壤结构中的表面流和地下流。水资源进展，2020年，144：103701。https://doi.org/10.1016/j.advwatres.2020.103701
[10] RIESTIANA V. A.，SETIYOWATI R.，和 KURNIAWAN V. Y. 使用有限差分法的一维浅水波浪方程的数值解：拉克斯-弗里德里希斯格式。AIP会议记录，2021年，2326：020022。https://doi.org/10.1063/5.0039545
[11] SETIYOWATI R. 使用有限体积法模拟浅水波浪方程：拉克斯-弗里德里希斯方案。物理学杂志：会议系列，2019，1306：012022。https://doi.org/10.1088/1742-6596/1306/1/012022
[12] PANTELAKIS D.、ZISSIS T.、ANASTASIADOU-PARTHENIOU E. 和 BALTAS E. 用于模拟地表灌溉系统内农田地表径流的数值模型。水资源管理，2012，26：1217-1229。https://doi.org/10.1007/s11269-011-9955-2
[13] RICHARDS L.A. 液体通过多孔介质的毛细管传导。应用物理学杂志，1931，1(5)：318-333。https://doi.org/10.1063/1.1745010
[14] LI Y., YUAN D., LIN B., 和 TEO F. Y. 地表水和地下水流的全耦合深度集成模型。水文学杂志，2016，542：172-184。https://doi.org/10.1016/j.jHydrol.2016.08.060
[15] BHUTTO A. A.、AHMED I.、RAJPUT S. A. 和 SHAH S. A. R. 振荡流对粘性磁流体动力磁流体动力学流体传热的影响。速度快数学学报，2023年，11(1)：1-16。https://doi.org/10.21015/vtm.v11i1.1386
[16] BHUTTO A. A.、SHAH S. F.、KHOKHAR R. B.、HARIJAN K. 和 HUSSAIN M. 研究障碍物配置对涡驱动燃烧不稳定性的影响。速度快数学学报，2023，11(1)：67-82。https://doi.org/10.21015/vtm.v11i1.1411
[17] KHOKHAR R. B.、BHUTTO A. A.、BHUTTO I. A.、MENGAL A.、SHAIKH F. 和 SHAIKH A. A. 通过带或不带多孔材料的环形空间的非牛顿流体流动的数值分析。俾路支省工程与应用科学杂志(北京电子学会)羟乙基纤维素于2023年获得“Y”类别认可。
[18] FLOURI E. T.、KALLIGERIS N.、ALEXANDRAKIS G.、KAMPANIS N. A. 和 SYNOLAKIS C. E. 有限差分计算模型在地震引发海啸模拟中的应用。应用数值数学，2013，67：111-125。https://doi.org/10.1016/j.apnum.2011.06.003
[19] 陆旭，董斌，毛斌，张旭。基于收敛改进的拉克斯-弗里德里希斯方案的数值方案及其在求解一层和两层浅水方程中的应用。工程数学问题，2015，2015：379281。https://doi.org/10.1155/2015/379281
[20] SAIDUZZAMAN M., & RAY S.K. 浅水方程数值方案的比较。全球科学前沿研究杂志：数学与决策科学，2013，13(4)：28-46。https://www.researchgate.net/profile/Sobuj-Ray/publication/258342122_Comparison_of_Numerical_Schemes_for_Shallow_Water_Equation/links/5882ff55a6fdcc6b790ef1b8/Comparison-of-Numerical-Schemes-for-Shallow-Water-Equation.pdf
[21] LU C., XIE L., 和 YANG H. 具有底部地形的浅水方程的简单有限体积拉克斯-温德罗夫加权本质上非振荡格式。工程数学问题，2018，2018，2652367。https://doi.org/10.1155/2018/2652367
[22] BING Y. U. A. N., JIAN S. U. N., YUAN D. K., 和 TAO J. H. 基于二维有限体积模型的浅水驱数值模拟. 流体动力学杂志，系列。乙, 2013, 25(4): 520-527. https://doi.org/10.1016/S1001-6058(11)60391-1
[23] ZOPPOU C., & ROBERTS S. 二维非稳定溃坝数值解。应用数学建模，2000, 24(7): 457-475。https://doi.org/10.1016/S0307-904X(99)00056-6
[24] RAJPUT S. A., KAMBOH S. A., AMUR K. B.,

MEMON S., 和 GHOTO A. A. 利用有限差分法对恒定外力作用下的二维浅水方程进行数值模拟。速度快数学学报，2023年，11(1)：170-179。https://doi.org/10.21015/vtm.v11i1.1469

[25] KAMBOH S. A.、SARBINI I. N.、LABADIN J. 和 EZE M. O. 使用MATLAB模拟明渠中的二维圣维南方程。亚洲IT杂志，2015，5(1)：15-22。https://doi.org/10.33736/jita.47.2015

[26] KIRSTETTER G., HU J., DELESTRE O., DARBOUX F., LAGRÉE P. Y., POPINET S., FULLANA J. M., 和 JOSSERAND C. 模拟降雨驱动的地表水流：浅水近似中的经验与解析摩擦项。水文学杂志，2016，536：1-9。https://doi.org/10.1016/j.jHydrol.2016.02.022

[27] GARCIA R., & KAHAWITA R.A. 使用麦科马克有限差分格式对圣维南特方程进行数值解。国际流体数值方法杂志，1986，6(5)：259-274。https://doi.org/10.1002/fld.1650060502

[28] AMIRI S. M.、TALEBBEYDOKHTI N. 和 BAGHLANI A. 浅水方程的二维良好平衡数值模型。伊朗科学，2013，20(1)：97-107。https://doi.org/10.1016/j.scient.2012.12.001

[29] ANASTASIOU K., & CHAN C. T. 在非结构化三角网格上使用有限体积法求解二维浅水方程。国际流体数值方法杂志，1997，24(11)：1225-1245。https://doi.org/10.1002/(SICI)1097-0363(19970615)24:11<1225::AID-FLD540>3.0.CO;2-D

[30] KURGANOV A. 浅水方程的有限体积方案。数值学报，2018，27：289-351。https://doi.org/10.1017/S0962492918000028

[31] NAMIO F. T.、NGONDIEP E.、NTCHANTCHO R. 和 NTONGA J. C. 带源项的完整浅水问题数学模型，拉克斯-温德罗夫方案的稳定性分析。理论与计算科学杂志，2015，2(4)：1000132。https://doi.org/10.4172/2376-130x.1000132

[32] 梁世杰, 唐建华, 吴明生. 最小二乘有限元法求解浅水方程. 力学学报, 2008, 24: 523-532. https://doi.org/10.1007/s10409-008-0151-4

[33] ALCRUDO F., & GARCIA-NAVARRO P. 二维浅水方程有限体积中的高分辨率戈杜诺夫型方案。国际流体数值方法杂志，1993，16(6)：489-505。https://doi.org/10.1002/fld.1650160604

[34] BRAND S. 浅水方程数值解的并行算法。捷克-日本应用数学研讨会论文集，布拉格，2006年，第 25-36 页。https://geraldine.fjfi.cvut.cz/cjs2006/proc/brand.pdf

[35] WAKJIRA G. T. 使用有限差分和有限体积方法的洪水传播模型数值解。博士论文，2017。